ISSN 0001-4338, Izvestiya, Atmospheric and Oceanic Physics, 2012, Vol. 48, No. 2, pp. 174–184. © Pleiades Publishing, Ltd., 2012.
Original Russian Text © E.G. Merzlyakov, Yu.I. Portnyagin, T.V. Solov'eva, A.I. Pogoreltsev, E.V. Suvorova, 2012, published in Izvestiya AN. Fizika Atmosfery i Okeana, 2012, Vol. 48, No. 2, pp. 195–206.

Altitude–Latitude Structure of the Vertical Wind Component of the Migrating Diurnal Tide in the Range of Heights from 80 to 100 km

E. G. Merzlyakov[a], Yu. I. Portnyagin[a], T. V. Solov'eva[a], A. I. Pogoreltsev[b], and E. V. Suvorova[b]

[a] *Typhoon Research and Production Association, ul. Pobedy 4, Obninsk, Kaluga oblast, 249038 Russia*
e-mail: eugmer@typhoon.obninsk.ru

[b] *Russian State Hydrometeorological University, Malookhtinskii pr. 98, St. Petersburg, 195196 Russia*

Received January 11, 2011; in final form, March 17, 2011

Abstract—Based on empirical monthly data on the parameters of oscillations in the horizontal wind component of the diurnal migrating tide, we calculated the altitude–latitude distributions of the parameters of oscillations in the vertical wind component of the diurnal tide in the region of the mesosphere and lower thermosphere (80–100 km). The initial data were obtained from satellite observations of the mesosphere and lower thermosphere at altitudes from 90 to 120 km and from data of ground-based sounding of this region using the radio meteor method and the method of partial reflections in the altitude range from 80 to 100 km. We compare the resulting distributions with the results of numerical modeling for the migrating diurnal tide using a global circulation model for the middle and upper atmosphere. It is shown that, accurate to measurement errors, there is a good agreement between the distributions of parameters of the migrating diurnal tide obtained by the models. One specific feature of the empirical distributions of the amplitude of the vertical wind oscillations is that there are three regions of increased amplitude values—in the vicinity of the equator and at 30° N and 30° S latitudes—which were observed for all seasons. The maximum value of the amplitude of the vertical wind oscillations is approximately 0.1 m/s. The divergence of the Eliassen–Palm flux was estimated to be on the order of 10 m s^{-1} day^{-1}.

Keywords: mesosphere, lower thermosphere, diurnal tide, vertical wind.

DOI: 10.1134/S0001433812020077

1. INTRODUCTION

In a previous paper [1], the authors constructed altitude–latitude distributions of the amplitudes and phases of vertical wind component oscillations caused by the semidiurnal migrating tide for typical seasons of the year: solstice and equinox periods. The vertical wind velocity was calculated using an empirical model of the horizontal wind component of the semidiurnal tide, which is based on data from long-term ground-based measurements of wind velocity carried out with the help of the radio-meteor method (MR radars) and the method of partial reflections (MF radars). This paper deals with the migrating diurnal tide, the main source of which is thermal heating due to the absorption of solar radiation by water vapor and ozone. Some characteristics of the altitude–latitude distributions of the parameters of the migrating diurnal tide for the horizontal wind velocity can be found in [2, 3], which analyzed data of ground-based radar measurements of wind velocity in the mesosphere and lower thermosphere (MLT). The peak amplitudes of tidal oscillations in the horizontal wind are observed at latitudes between 20° and 30° in both hemispheres, where the migrating diurnal tide is the main large-scale regular oscillation. The main modes of the diurnal tide are the mode (1, 1), which corresponds to the vertically propagating tide at low latitudes, and the evanescent mode (1, –1) [4]. The evanescent mode is concentrated in high latitudes and manifests itself at altitudes above 90 km [2]. The seasonal course of the amplitudes of oscillations in the horizontal wind velocity caused by the diurnal migrating tide is characterized by peaks during spring and fall equinoxes.

Earlier (see, for example, [3, 4]) it has been shown that the amplitudes and phases of the diurnal tide obtained from data of MF radars starting from heights of 85–90 km are considerably different from their values determined from satellite and MR-radar observations in mid- and low latitudes. No general rule to correct MF-radar data was found. For different measurement stations located at different longitudes and latitudes, the ratios of tidal parameters obtained from MF- and MR-radar data in nearly the same area are different. Therefore, we used satellite data to construct an empirical model of diurnal tides above 90 km. To this end, we used measurement data on the horizontal component of wind velocity obtained with the Wind Imaging Interferometer (WINDII), onboard the Upper Atmosphere Research Satellite (UARS) [5].

In this paper we consider semi-empirical altitude–latitude distributions of parameters of oscillations in the vertical wind component caused by the migrating diurnal tide for the main seasons of the year. Section 2 discusses the results of a numerical simulation of a migrating diurnal tide using a mechanistic model of the upper atmospheric circulation. Section 3 describes the empirical model of horizontal wind (required for calculating the vertical wind velocity) based on the results of long-term measurements of the horizontal wind velocity in the network of MF and MR radars and WINDII measurement data. Section 4 describes the results of semi-empirical simulations of the vertical diurnal tidal wind on the basis of the horizontal wind model described in Section 3. Section 5 compares the results of numerical and semi-empirical simulations of diurnal vertical winds. This section also compares data on the altitude–latitude structure of diurnal vertical winds and data on the corresponding temperature distributions. The conclusions are made in Section 6.

2. NUMERICAL MODEL OF DIURNAL TIDAL WIND AND TEMPERATURE IN THE UPPER ATMOSPHERE

The parameters of tidal oscillations of the vertical wind and temperature were numerically calculated using the Middle and Upper Atmosphere Model (MUAM). A brief description of this model and specific features of the numerical calculations can be found in [1]. A detailed description of the numerical experiments can be found in [6]. In view of this, we turn to the numerical results, which should be regarded as long-term monthly averages.

Figure 1 shows the distributions of amplitude and phase (time of maximum) of oscillations in the meridional wind component for the period of the vernal equinox (March). In the MLT region, the oscillations are concentrated mainly in low latitudes. The value of the amplitude reaches up to 35 m/s. The phase distribution testifies that the tide propagation is bottom-up with a vertical wavelength of around 30 km in the log-isobaric coordinate system.

Figure 2a shows the altitude–latitude distribution of the amplitude of oscillations in the vertical wind component for the diurnal migrating tide based on the results of numerical modeling of the circulation for March conditions. The main structures in these distributions are the areas of peak amplitude values near the equator and the secondary maximums of the amplitude at low latitudes. In the equatorial area, the maximum amplitude values of up to 0.12 m/s are typical for heights of 80–100 km. Two other local maximums are located nearly at the 30° S and 30° N latitudes.

To turn to wind velocity distributions corresponding to the fall equinox, it is necessary to swap the hemispheres; in this case, the meridional wind phase is shifted by 12 h, and, for example, for the Northern Hemisphere, the phase of maximum in the meridional wind component of the diurnal tide is approximately the same throughout the year. For the phase of maximum in the vertical wind component, there is no need for a phase change after hemispheric swapping.

In [1] the authors introduced the concept of an "equivalent" vertical wind for the migrating semidiurnal tide. This term is based on the relation between complex amplitudes of oscillations in temperature and vertical wind for tides in the absence of sources and sinks of oscillations in a horizontally homogeneous windless atmosphere. For the semidiurnal migrating tide, the velocities of the "equivalent" vertical wind and the actual vertical wind turned out to be close to one another. Thus, one can use simple transformations to turn from temperature oscillations to oscillations in vertical wind. The numerical calculations show that, for the migrating diurnal tide in the MLT, the distributions of amplitudes of the "equivalent" vertical wind and true vertical wind are also similar, although there is no a close proximity as in the case of the semidiurnal tide. At altitudes above 110 km and below 80 km, there are significant differences that are caused by a thermal source of diurnal oscillations at these altitudes. Figure 2b shows the results of numerical calculations of the amplitude and phase of the diurnal oscillations in temperature scaled to the "equivalent" vertical wind. Thus, for the MLT region (80–100 km), one can use calculations of the parameters of oscillations in the vertical wind to estimate the parameters of the diurnal temperature oscillations. This will be used by us hereafter for approximate calculations of the Eliassen–Palm fluxes and flux divergence.

3. EMPIRICAL MODEL OF DIURNAL OSCILLATIONS IN HORIZONTAL WIND VELOCITY IN THE MLT REGION

To construct a model of diurnal tidal variations of the horizontal wind, we used the results of long-term measurements of the horizontal wind component on a network MR and MF radars. This network consists of 35 stations located at different longitudes and latitudes of the Northern and Southern hemispheres. All stations provide information on the vertical profile of the horizontal wind component. The data were obtained at different stations and in different time periods (mainly 1990–2003 measurement data were used). The height–latitude distributions for each wind component were constructed using the same method as in [1]. The difference is that the ground-based data were used to construct the model distributions up to an altitude of 90 km. In the layer between 90 and 95 km, the resulting model distributions of tidal parameters were

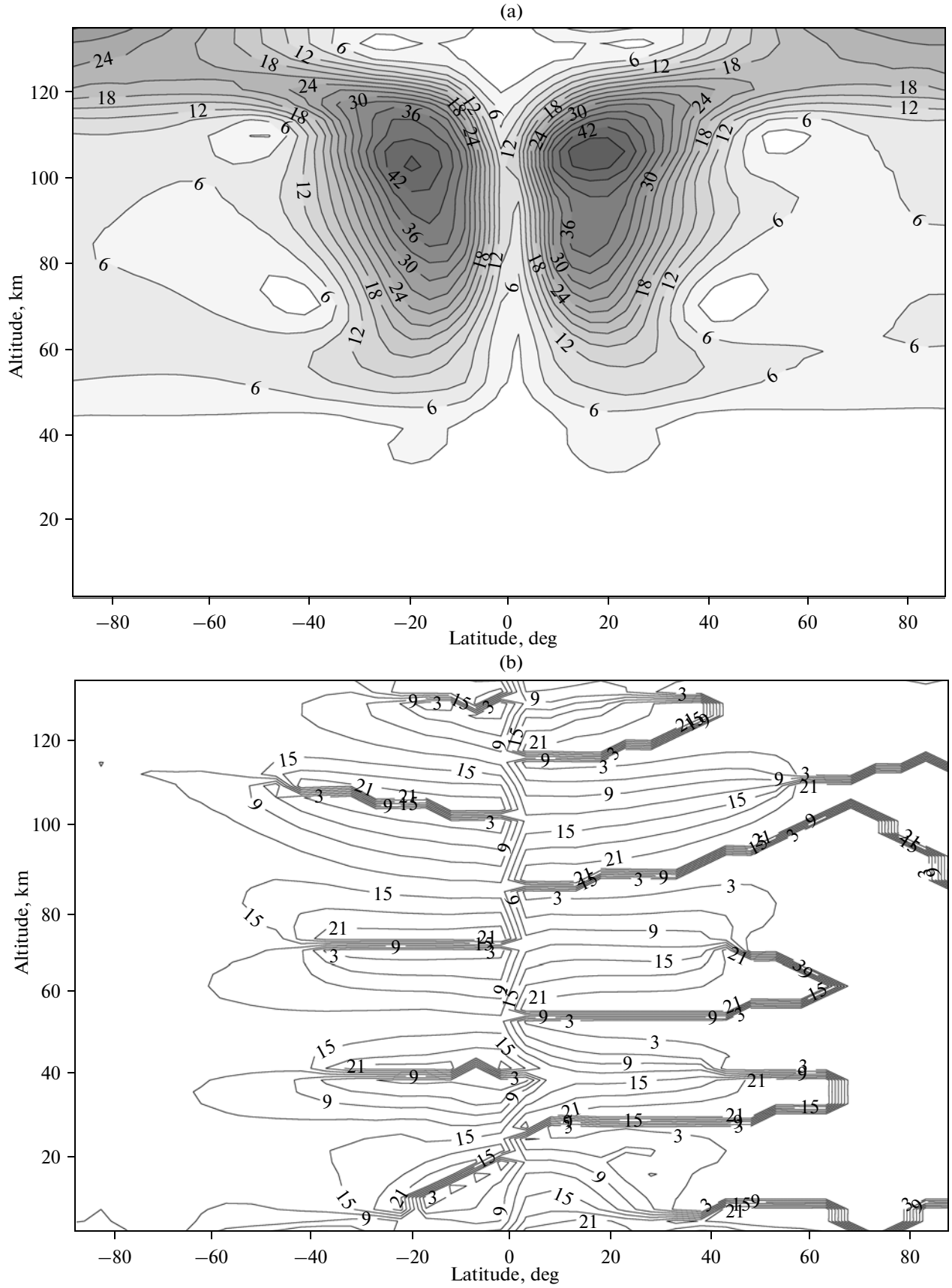

Fig. 1. Distribution of (a) amplitude and (b) phase (time of maximum) of the meridional wind oscillations for vernal equinox (March).

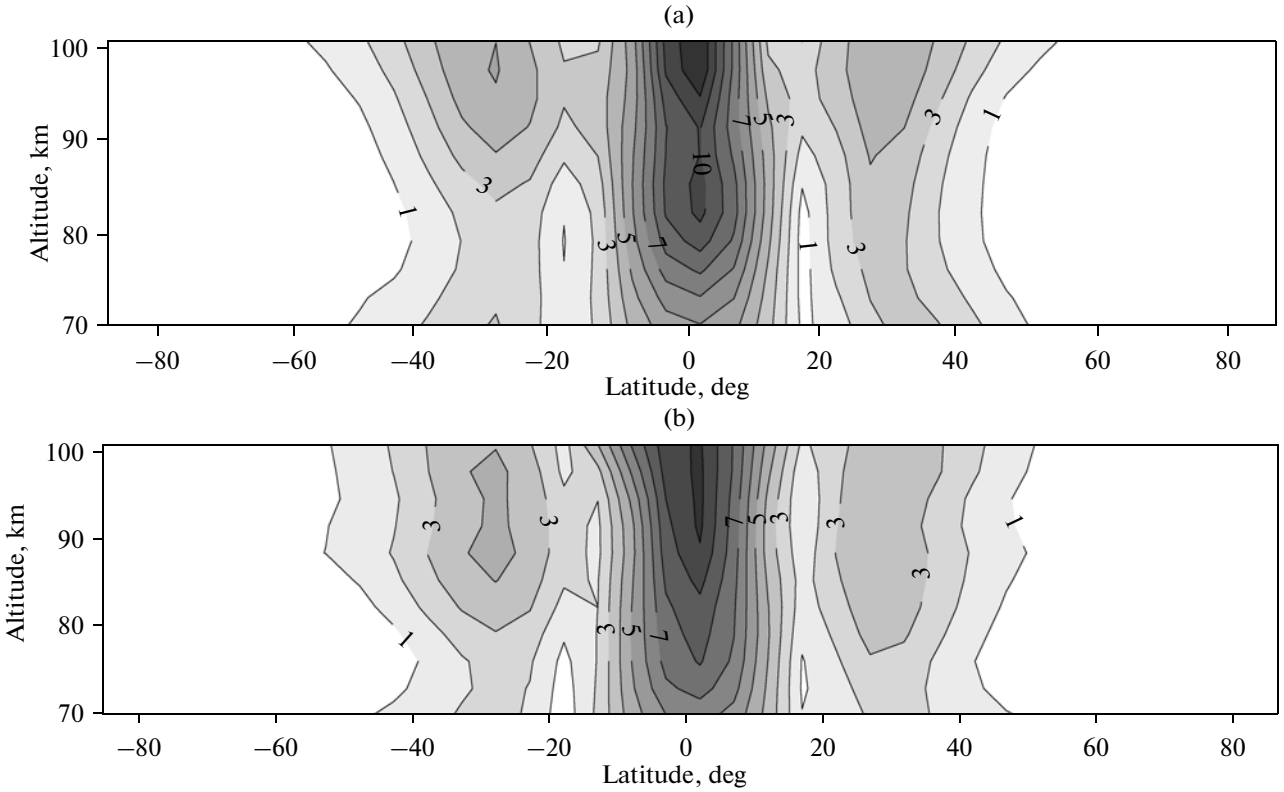

Fig. 2. (a) Altitude–latitude distribution of amplitude of vertical wind (cm/s) for the diurnal migrating tide by the results of numerically modeling circulation for March. (b) Same as (a) except for the amplitude of the "equivalent" vertical wind.

merged with empirical model distributions of parameters of diurnal oscillations in horizontal wind obtained in [5] from satellite measurement data by a two-dimensional interpolation technique described in [1]. This model covers a latitude range from 80° S to 80° N; therefore, the resulting semi-empirical model also covers this latitudinal range and extends to 120 km in altitude. Additionally, we note that, in the Southern Hemisphere for latitudes higher than 68°, a model of a migrating diurnal tide described in [7] was used. Figure 3 shows the altitude profiles of the amplitudes and phases of diurnal tide at latitudes of 30° S and 30° N derived in accordance with both models. In the vicinity of 90 km, where the models overlap, the values of the amplitudes and phases of diurnal tides in these two models agree accurate to measurement errors. However, at altitudes above 90 km, the amplitude values according to MF-radar data are significantly different from the values of satellite measurement data. The agreement in the vicinity of 90 km makes it possible to combine the models based on the results of ground-based (MF and MR radars) and satellite (WINDII) observations in this range.

The weighting coefficients were chosen so that $\sigma_{lat} = 7.5°$, $\sigma_h = 2$ km, where σ_{lat} and σ_h are the standard deviations of the weighting function with respect to latitude and height, respectively. For model altitude–latitude distributions of the tidal parameters, the longitude of the stations was ignored. Thus, we actually perform averaging in longitude at a fixed solar local time to retain only the migrating tide.

As was mentioned above, the ground-based data were obtained at different stations for different years, but the measurement period for each station is at least three years. The difference in the number of years introduces an additional random error into the long-term average values, which also have an error because of wind measurement inaccuracies. To assess the effect of different averaging variants on errors, we used the longest data series for northern and southern latitudes and compare long-term averaged values obtained over the full series with three-year averages.

The gross error of model amplitudes (with measurement errors) constituted 5 to 10 m/s for ground-based data. The model values of the tidal phase have a random error reaching 4 h. In addition to the measurement-induced error, the model distributions of the diurnal tide amplitude and phase constructed from ground-based data are also characterized by an error in the model construction method. This error arises

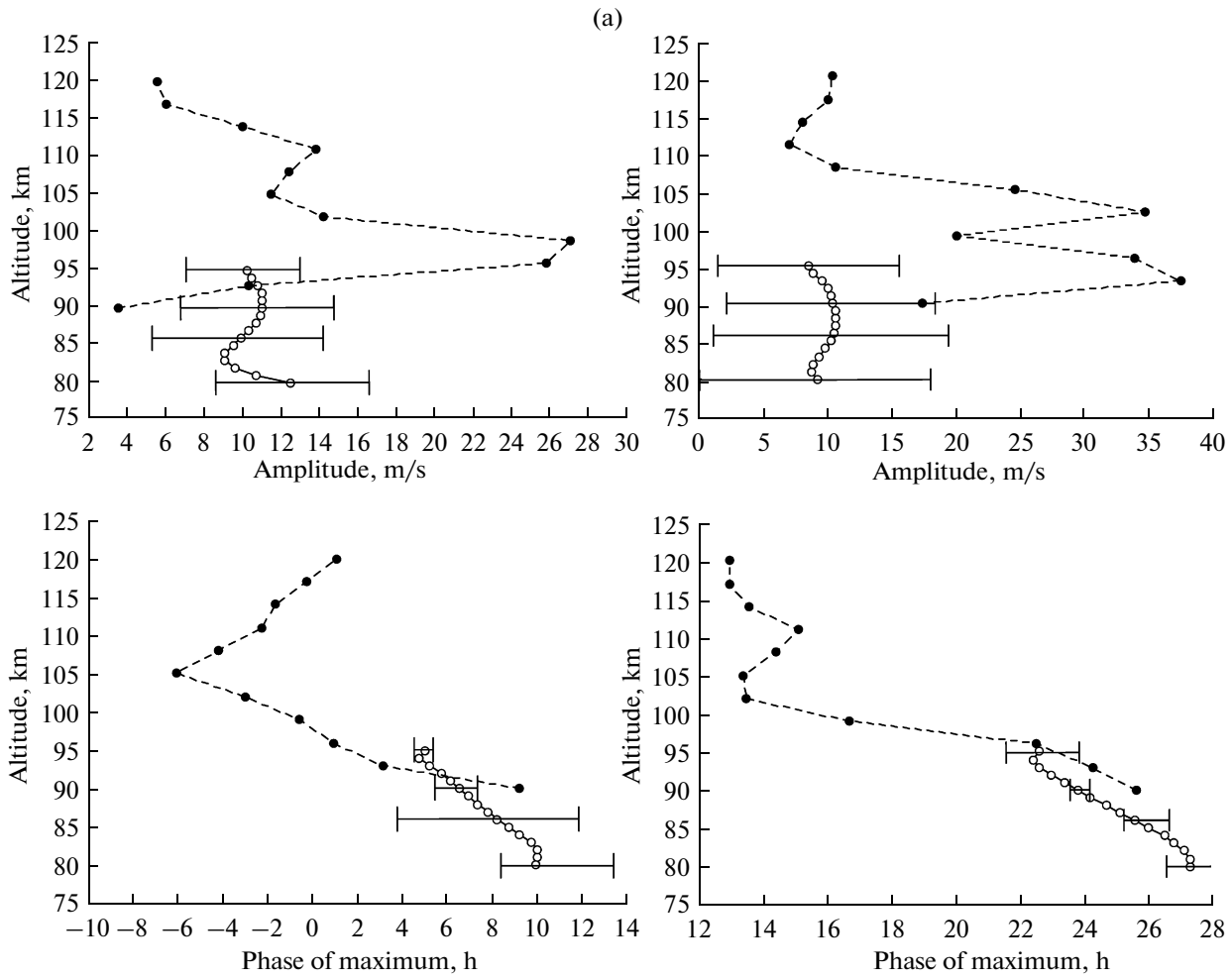

Fig. 3. (a) Altitude profiles of amplitudes and phases of the zonal (left) and meridional (right) wind components of the diurnal tide in March from ground-based observation data and by the WINDII model for 30° N. (b) Same as (a) except for 30° S.

from the incomplete averaging of nonmigrating tides over longitude because the stations are nonuniformly distributed by longitudes. To estimate the systematic error, we used the parameters of nonmigrating tides obtained in [7]. Based on these data, for each station one can calculate the hourly average wind velocity caused by the main nonmigrating diurnal tides. Then, instead of real data on the diurnal tide, one takes the diurnal tide parameters calculated from the values of wind velocity due to the nonmigrating tides and constructs model distributions in line with the abovementioned technique. The systematic error in some limited regions reaches 14 m/s (0°–10° S and 20°–30° S at a height of 85 km) and, on average, is 5–6 m/s.

The diurnal tide parameters derived from satellite data contain no systematic error. The random error of the amplitude of oscillations in the horizontal wind velocity speed is approximately 3 m/s, and the phase error in an area with high amplitude values (~20 m/s) is around 2.5 h.

Figure 4 shows the altitude–latitude distributions of the amplitudes and phases of the meridional wind component of the migrating tide derived from satellite and ground-based observations for the solstice and equinox periods. The high-amplitude areas are located nearly symmetric with respect to the equator close to 20° S and 20° N latitudes. The phase distribution corresponds to the bottom-up tide propagation. The vertical wavelength is around 20–25 km in low latitudes. Above 110 km, large diurnal tide amplitudes are observed in high latitudes. Here, the vertical wavelength of the diurnal tide exceeds the vertical dimensions of the MLT region, which corresponds to the appearance of the evanescent mode of the diurnal tide. This mode reaches its peak amplitude in the summer hemisphere at an altitude of around 110 km.

(b)

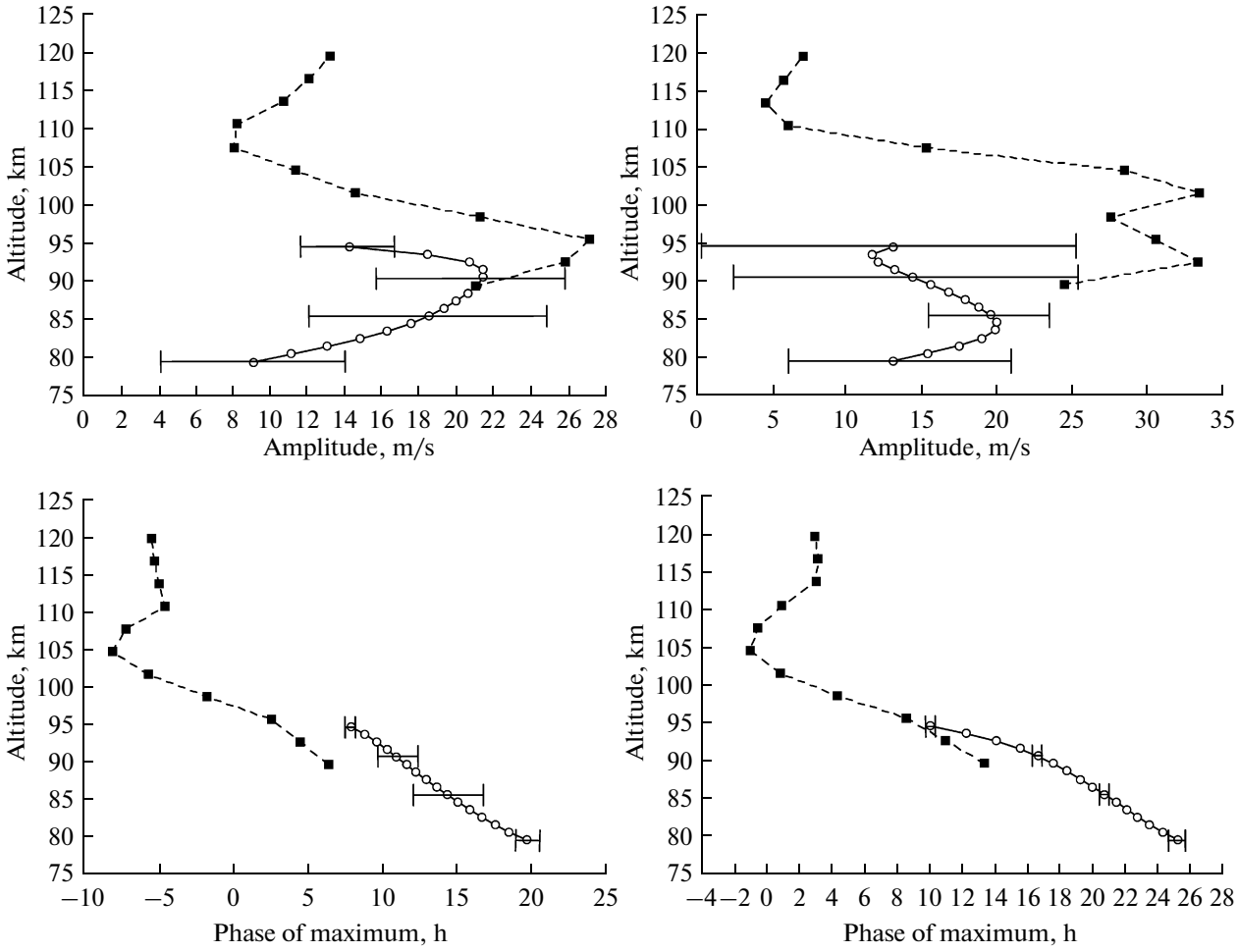

Fig. 3. Contd.

4. SEMI-EMPIRICAL ALTITUDE–LATITUDE DISTRIBUTIONS OF PARAMETERS OF DIURNAL OSCILLATIONS IN THE VERTICAL WIND

The tidal vertical wind is calculated using the following equation:

$$\frac{1}{a}\frac{\partial u}{\partial \lambda} + \frac{1}{a\cos\varphi}\frac{\partial}{\partial \varphi}(v\cos\varphi) + \frac{1}{\rho_0}\frac{\partial(\rho_0 w)}{\partial z} = 0, \qquad (1)$$

where u, v, and w are the wind components in the zonal, meridional, and vertical directions, respectively (the positive directions are the eastern, northern, and upward directions, respectively); a is the earth's radius, φ is the latitude, λ is the longitude, and $\rho_0 = \exp(-z/H)$. Equation (1) was written in the log-baric coordinate system $z = -H\ln(p/p_0)$, where $H = 7$ km, p is the pressure, and p_0 is the pressure at the lower boundary (surface). The equation is integrated top down. At the upper boundary of the model, zero boundary values of w are specified. The solution "forgets" the boundary conditions at a distance of less than 10 km from the upper boundary.

The above-described errors in the parameters of horizontal tidal wind are translated according to Eq. (1) into errors in the parameters of vertical wind. The random error in the amplitude is approximately 0.01 m/s, and the systematic error in the amplitude constitutes 0.02–0.06 m/s. The calculated values are considered significant if the magnitude of the amplitude exceeds the error. For the systematic error, we can obtain only an approximate estimate for its magnitude and distribution by latitude and altitude.

Figure 5 shows the altitude–latitude distributions of the amplitude and phase of the vertical wind component for the periods of solstice (December) and equinox (March). The areas of significant amplitude values are marked in shades of gray. In all seasons these

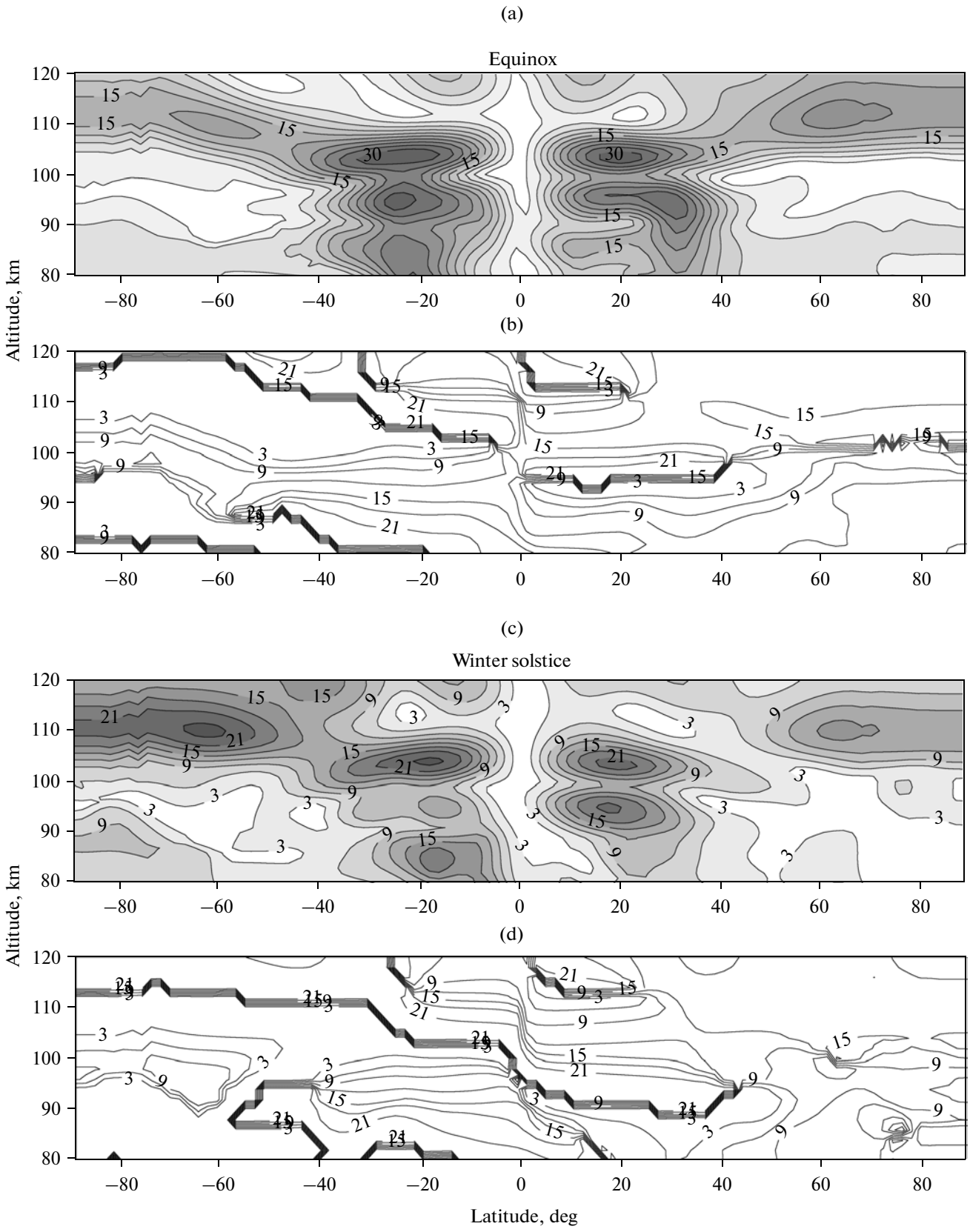

Fig. 4. Altitude–latitude distributions of the amplitude (m/s) and phase (h) of the meridional wind component of the migrating diurnal tide for (a, b) the period of the March equinox and (c, d) the period of December solstice.

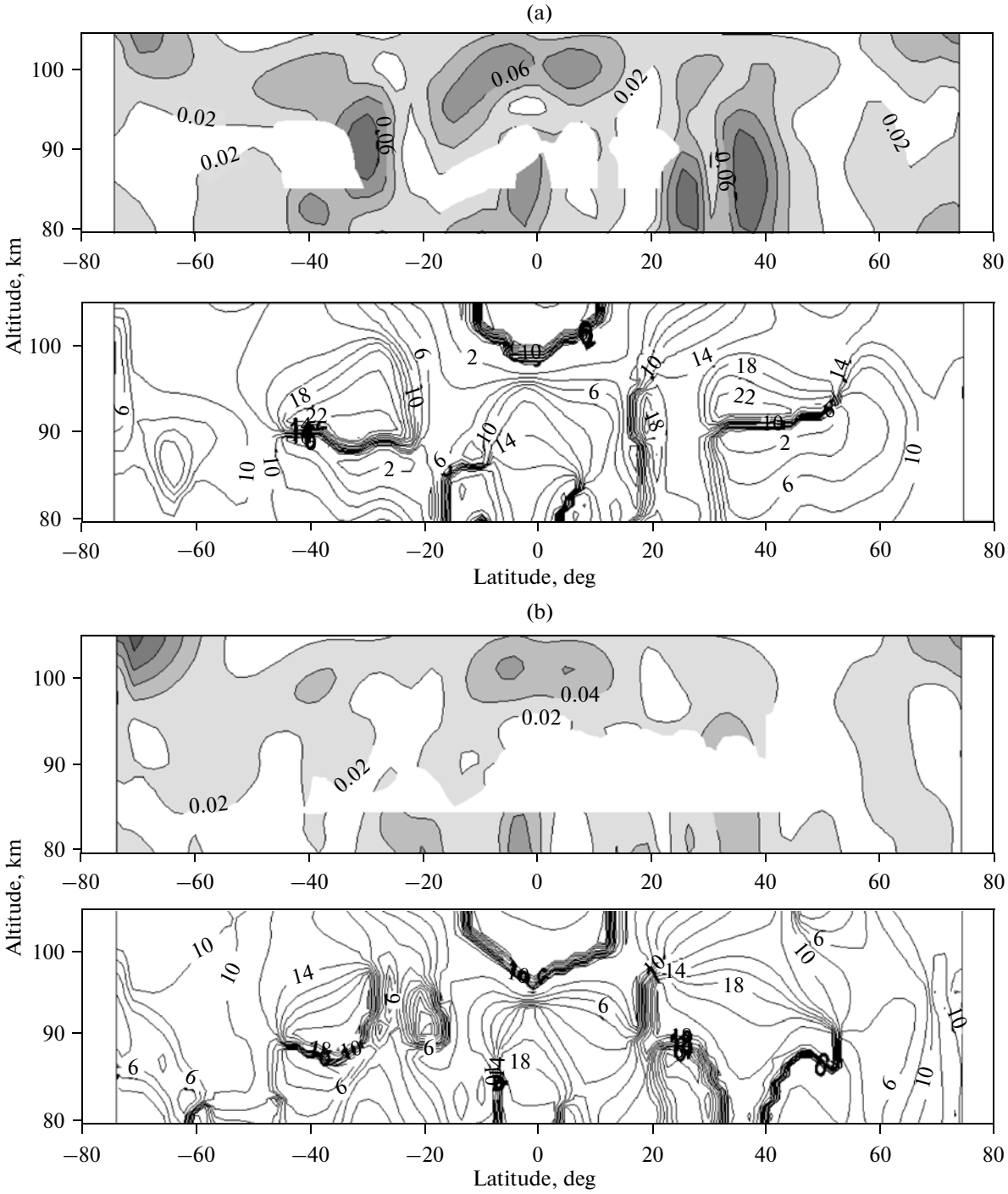

Fig. 5. Same as Fig. 4 except for the vertical wind component.

distributions involve clearly seen latitudinal zones of high amplitudes near the equator and in the vicinity of 30° S and 30° N. In December, another high-amplitude zone is seen in the polar region of the Southern Hemisphere at altitudes of at least 100 km. As was mentioned earlier, this is the evanescent diurnal tide in the summer hemisphere. The maximum values of the amplitude of vertical wind oscillations are around 0.08 m/s.

Based on the 2002–2008 satellite measurements of temperature, the authors of [8] calculated the height–latitude distributions of the parameters of tidal oscillations in the vertical wind. The resulting distributions

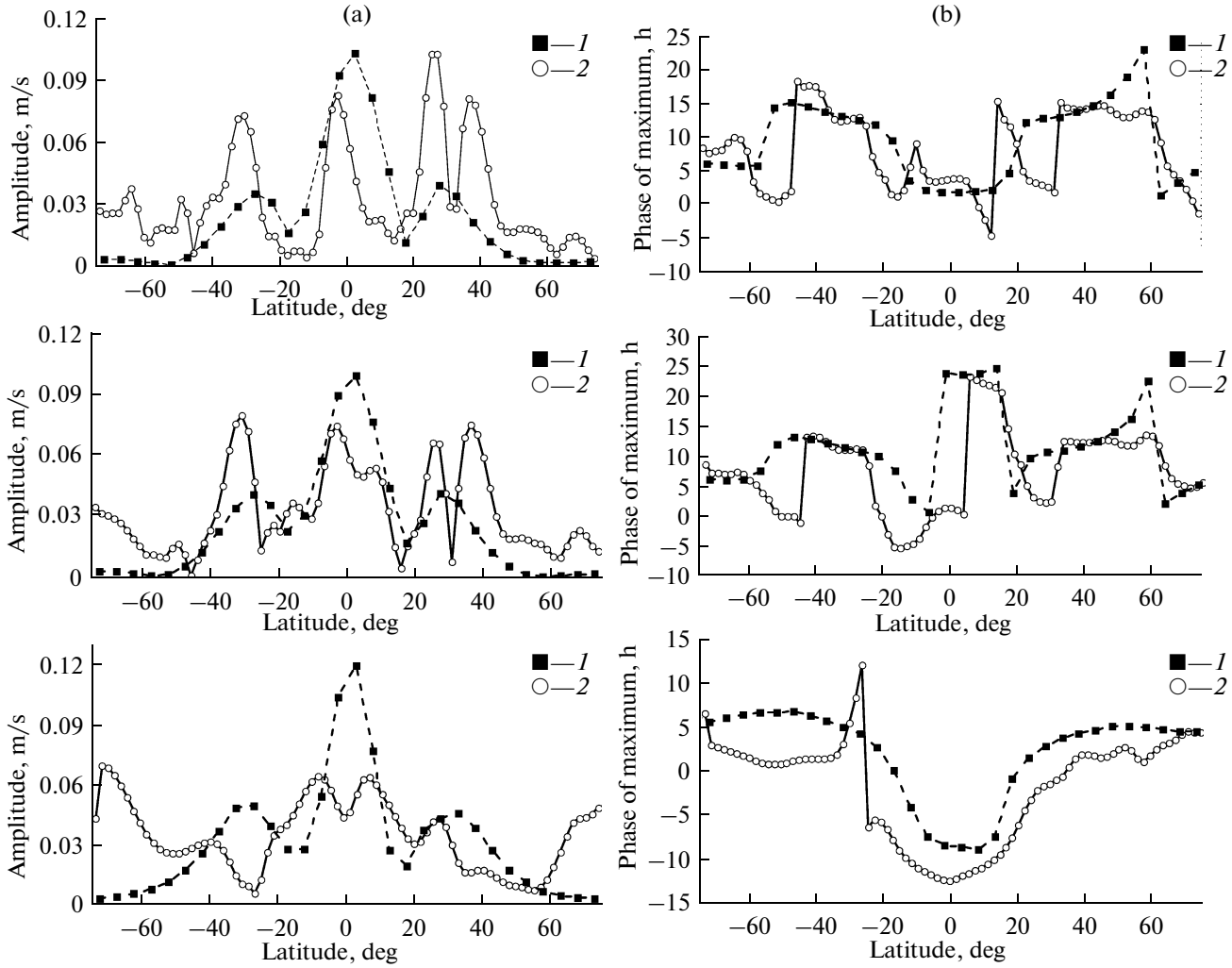

Fig. 6. (a) Amplitude of diurnal vertical wind oscillations as a function of latitude according to numerical calculations (*1*) and the semi-empirical model (*2*) in March at heights of (top to bottom) 86, 90, and 100 km. (b) Same as (a) except for the phase of diurnal oscillations.

are characterized by areas of increased amplitude values similar to those obtained in the present work.

5. DISCUSSION OF RESULTS

Figure 6 shows a comparison of the results of a numerical simulation of atmospheric circulation with the MUAM model and the results of semi-empirical calculations described in chapters 3 and 4. Figure 6a shows the dependence of the amplitudes of diurnal vertical wind oscillations on latitude at heights of 86, 90, and 100 km obtained from numerical calculations and semi-empirical modeling data for March. Figure 6b shows the corresponding distributions for the phase of vertical wind oscillations. It is noteworthy that the distributions of oscillation amplitudes in low and mid latitudes are very consistent, although there is a slight difference in the location of maximums and the absolute values of amplitudes. In the semi-empirical model of the migrating diurnal tide, the amplitude distribution by latitude is more complex than the distribution obtained by MUAM. Primarily this is caused by the extent to which the numerical model takes into account sources of variation in tidal amplitude oscillations. On the other hand, the empirical model is based on data averaged over several years. The diurnal tide in the MLT region is subjected to the quasi-biennial variations, and their incomplete averaging may lead to both a large error in the values of model tidal parameters (this error has been described earlier) and to changes in the altitude–latitude distributions of model parameters.

An analysis of the altitude–latitude structure of phases of the vertical wind oscillations for different seasons by data of different methods shows that these structures are similar in areas with large amplitudes. These areas are characterized by a regular phase change in height corresponding to the vertical propa-

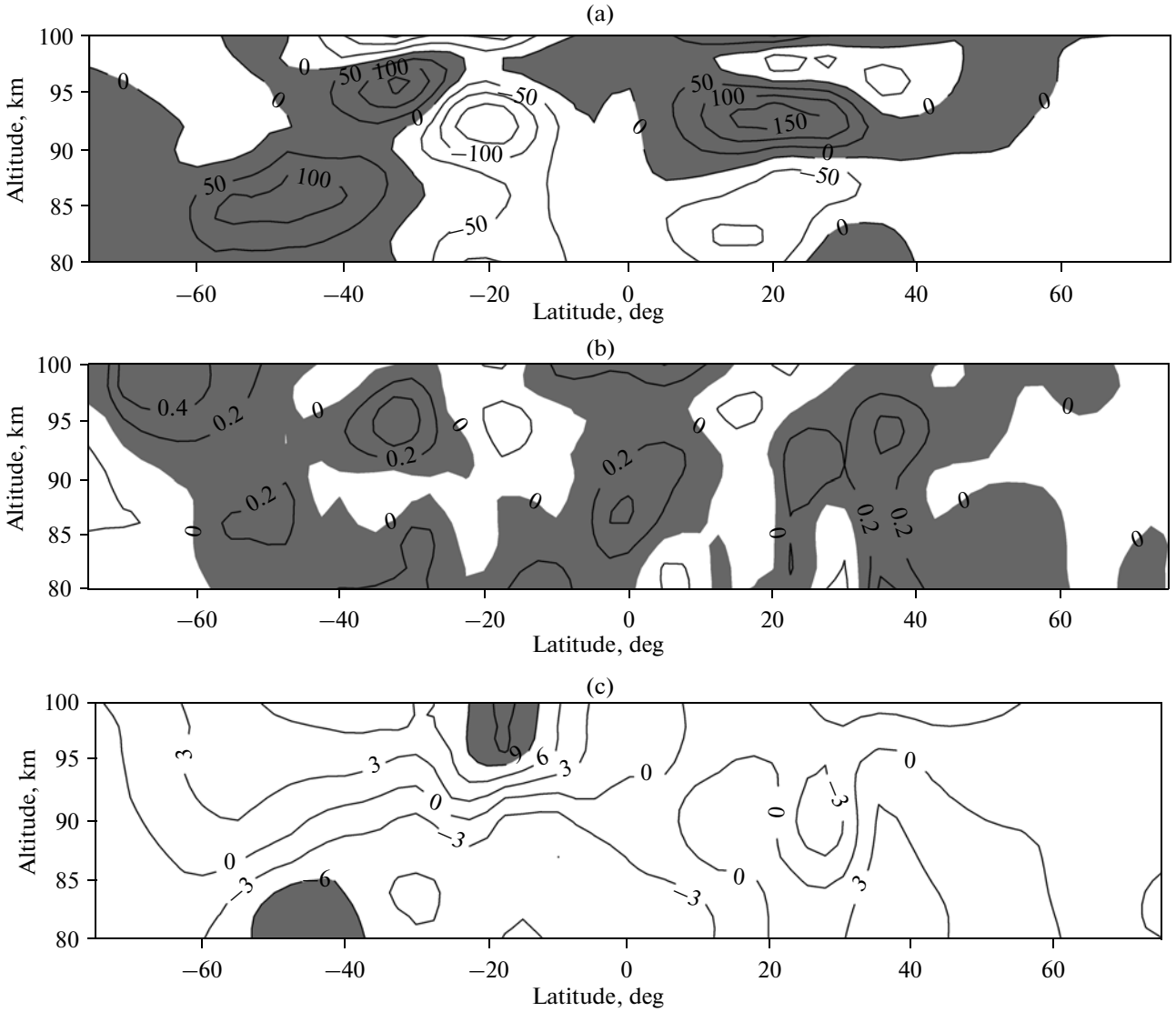

Fig. 7. Altitude–latitude distributions of (a) horizontal and (b) vertical components of the Eliassen–Palm flux (m^2/s^2) and (c) its divergence (m s^{-1} day^{-1}) for March. The areas with positive flux components and statistically significant values of the flux divergence are highlighted in gray.

gation of oscillations. In general, numerical and observation-based calculations yield consistent distributions for parameters of diurnal vertical wind oscillations.

Based on the results of numerical simulations, we have concluded that the "effective" vertical wind is consistent with the true vertical wind. This allows us to estimate the parameters of diurnal temperature oscillations on the basis of parameters of diurnal vertical wind oscillations calculated from experimental data. In turn, this makes it possible to calculate the semiempirical heat and momentum fluxes associated with the migrating diurnal tide and estimate the zonal flow accelerations. Figure 7 shows the altitude–latitude distributions of the meridional and vertical components of the Eliassen–Palm flux and zonal flow acceleration (m s^{-1} day^{-1}), which is induced by the diurnal tide in the atmosphere in March. The statistically significant value (higher than the rms error) is approximately 10 m s^{-1} day^{-1}. Note that the vertical component of the Eliassen–Palm flux is smaller than its horizontal component. This explains the fact that, according to the numerical simulation, the residual circulation [9] and the circulation defined in terms of Euler variables have no significant differences. The estimates for the Eliassen–Palm flux divergence obtained by us are consistent with the results of [10, 11], which used different wind and temperature measurement data. The emerging zonal flows are torqued by the Coriolis force and lead to a change in the prevailing meridional wind, which eventually results in a cellular structure in the altitude–latitude circulation.

5. CONCLUSIONS

This paper presents the altitude–latitude distributions of the amplitude and phase of the vertical wind oscillations caused by the migrating diurnal tide. The calculations were performed using an empirical model of diurnal oscillations of horizontal in the MLT region. In constructing the model distributions of parameters of the horizontal wind oscillations, we took into account the specific features of MF-radar data. This made it possible to substantially improve these distributions in comparison with [12], where the amplitudes of diurnal horizontal wind oscillations are too small and the vertical wavelength is too large in comparison with the values corresponding to most recent experimental data.

The migrating diurnal tide was numerically simulated using a global circulation model of the middle and upper atmosphere. The results of numerical calculations are qualitatively and quantitatively consistent with the results obtained from satellite and ground-based observation data. The MUAM model yields the same main structures of tidal oscillations in the horizontal and vertical wind as the semi-empirical model. The amplitudes of horizontal wind oscillations are consistent with one another, reaching values of 35 m/s for the meridional component and 25 m/s for the zonal component. The vertical wind component obtained by a numerical simulation was twice as large. The amplitude of the vertical wind oscillations constituted approximately 0.06 m/s according to empirical modeling. The maximum amplitudes at altitudes of 80–100 km are observed in the latitudinal belts of 20°–40° in both hemispheres and over the equator. At altitudes above 90 km, the high-amplitude areas are overlapped with areas of high amplitudes of the semidiurnal tide. Here one should expect strong diurnal variations in the vertical wind. During measurements that do not cover a whole day (for example, nocturnal measurements of temperature), the seasonal course of a measured quantity will be coupled with the seasonal course of tidal amplitudes, which is important for data interpretation [13].

The calculated accelerations of the zonal mean flow generated by the diurnal tide in the MLT region reach values of 10 m s^{-1} day^{-1}.

ACKNOWLEDGMENTS

This work was supported by the Russian Foundation for Basic Research, project no. 08-05-00710. The authors are grateful to Dr. J. Oberheide for permission to use nonmigrating tidal analysis data and to a reviewer for useful comments.

REFERENCES

1. Yu. I. Portnyagin, E. G. Merzlyakov, T. V. Solov'eva, A. I. Pogorel'tsev, E. V. Suvorova, P. Mukhtarov, and D. Pancheva, "Height–Latitude Structure of the Vertical Component of the Migrating Semidiurnal Tide in the Upper Mesosphere and Lower Thermosphere Region," Izv. Akad. Nauk, Fiz. Atmos. Okeana **47** (1), 1–11 (2011).
2. Y. I. Portnyagin, T. V. Solovjova, N. A. Makarov, E. G. Merzlyakov, A. H. Manson, C. E. Meek, W. Hocking, N. Mitchell, D. Pancheva, P. Hoffmann, W. Singer, Y. Murayama, K. Igarashi, J. M. Forbes, S. Palo, C. Hall, and S. Nozawa, "Monthly Mean Climatology of the Prevailing Winds and Tides in the Arctic Mesosphere/Lower Thermosphere," Ann. Geophys. **22** (10), 3395–3410 (2004).
3. D. Pancheva, P. Mukhtarov, and B. Andonov, "Reply To Comment on 'Global Structure, Seasonal and Interannual Variability of the Migrating Semidiurnal Tide Seen in the SABER/TIMED Temperatures (2002–2007)' by Manson et al. (2010)," Ann. Geophys. **28**, 677–685 (2010).
4. S. Chapman and R. Lindzen, *Atmospheric Tides* (Springer, New York, 1969; Mir, Moscow, 1972).
4. Ch. Jacobi, C. Arras, D. Kürschner, W. Singer, P. Hoffmann, and D. Keuer, "Comparison of Mesopause Region Meteor Radar Winds, Medium Frequency Radar Winds and Low Frequency Drifts Over Germany," Adv. Space Res. **43** (2), 247–252 (2009).
5. D. Y. Wang, C. McLandress, E. L. Fleming, W. E. Ward, B. Solheim, and G. G. Shepherd, "Empirical Model of 90–120 km Horizontal Winds from Wind-Imaging Interferometer Green Line Measurements in 1992–1993," J. Geophys. Res. **102** (D6), 6729–6745 (1997).
6. A. I. Pogorel'tsev, "Generation of Normal Atmospheric Modes by Stratospheric Vacillations," Izv. Akad. Nauk, Fiz. Atmos. Okeana **43** (4), 463–475 (2007).
7. D. J. Murphy, J. M. Forbes, R. L. Walterscheid, M. E. Hagan, S. K. Avery, T. Aso, G. J. Fraser, D. C. Fritts, M. J. Jarvis, A. J. McDonald, D. M. Riggin, M. Tsutsumi, and R. A. Vincent, "A Climatology of Tides in the Antarctic Mesosphere and Lower Thermosphere," J. Geophys. Res. **111**, D23104 (2006).
8. J. Oberheide, Q. Wu, T. L. Killeen, M. E. Hagan, and R. G. Roble, "Diurnal Nonmigrating Tides from TIMED Doppler Interferometer Wind Data: Monthly Climatologies and Seasonal Variations," J. Geophys. Res. **111**, A10S03 (2006). doi 1029/2005JA011491.
9. D. G. Andrews, J. R. Holton, and C. B. Leovy, *Middle Atmosphere Dynamics* (Academic Press, London, 1987).
10. X. Zhu, J.-H. Yee, E. R. Talaat, M. Mlynczak, and J. M. Russell, "Diagnostic Analysis of Tidal Winds and the Eliassen–Palm Flux Divergence in the Mesosphere and Lower Thermosphere from TIMED/SABER Temperatures," J. Atmos. Sci. **65** (12), 3840–3859 (2008).
11. R. Liberman, "An Estimate of the Momentum Deposition in the Lower Thermosphere by the Observed Diurnal Tide," J. Atmos. Sci. **51** (20), 3094–3105 (1994).
12. Yu. Portnyagin, "A Review of Mesospheric and Lower Thermosphere Models," Adv. Space Res. **38** (11), 2452–2460 (2006).
13. S. P. Zhang and G. G. Shepherd, "The Influence of the Diurnal Tide on the $O(^1S)$ and OH Emission Rates Observed by WINDII on UARS," Geophys. Res. Lett. **26** (4), 529–532 (1999).